AGU ADVANCING EARTH AND SPACE SCIENCE

Geophysical Research Letters

RESEARCH LETTER
10.1029/2020GL091411

Special Section:
Fire in the Earth System

The 2019–2020 Australian Drought and Bushfires Altered the Partitioning of Hydrological Fluxes

Sujay V. Kumar[1], Thomas Holmes[1], Niels Andela[2], Imtiaz Dharssi[3,4], Vinodkumar[3,4], Christopher Hain[5], Christa Peters-Lidard[6], Sarith P. Mahanama[7,8], Kristi R. Arsenault[1,9], Wanshu Nie[10,11], and Augusto Getirana[1,9]

[1]Hydrological Sciences Laboratory, NASA GSFC, Greenbelt, MD, USA, [2]School of Earth and Ocean Sciences, Cardiff University, Cardiff, UK, [3]Bureau of Meteorology, Melbourne, Australia, [4]Bushfire and Natural Hazard Cooperative Research Centre, Melbourne, Australia, [5]Short-term Prediction Research and Transition Center, NASA MSFC, Huntsville, AL, USA, [6]Earth Science Division, NASA GSFC, Greenbelt, MD, USA, [7]Science Systems and Applications Inc., Lanham, MD, USA, [8]Global Modeling and Assimilation Office, NASA GSFC, Greenbelt, MD, USA, [9]Science Applications International Corporation, McLean, VA, USA, [10]Department of Earth and Planetary Sciences, Johns Hopkins University, Baltimore, MD, USA, [11]NASA Goddard Earth Sciences Technology and Research (GESTAR), Greenbelt, MD, USA

Key Points:

- Soil Moisture Active Passive vegetation optical depth (VOD) detects features of the 2019–2020 Australian bushfires and drought
- VOD assimilation improves land surface states and fluxes
- The vegetation changes from the 2019 to 2020 Australian fires and drought causes significant changes in the water budget partitioning

Supporting Information:

- Supporting Information S1
- Supporting Information S2

Correspondence to:
S. V. Kumar,
Sujay.V.Kumar@nasa.gov

Citation:
Kumar, S. V., Holmes, T., Andela, N., Dharssi, I., Vinodkumar, Hain, C., et al. (2021). The 2019–2020 Australian drought and bushfires altered the partitioning of hydrological fluxes. *Geophysical Research Letters*, *48*, e2020GL091411. https://doi.org/10.1029/2020GL091411

Received 27 OCT 2020
Accepted 8 DEC 2020

Abstract Though coarse in spatial resolution, the nearly all weather measurements from passive microwave sensors can help in improving the spatio-temporal coverage of optical and thermal infrared sensors for monitoring vegetation changes on the land surface. This study demonstrates the use of vegetation optical depth (VOD) retrievals from the Soil Moisture Active Passive mission for capturing the vegetation alterations from the recent 2019 to 2020 Australian bushfires and drought. The impact of vegetation disturbances on terrestrial water budget is examined by assimilating the VOD retrievals into a dynamic phenology model. The results demonstrate that assimilating VOD observations lead to improved simulation of evapotranspiration, runoff, and soil moisture states. The study also demonstrates that the vegetation changes from the 2019 to 2020 Australian drought and fires led to significant modifications in the partitioning of evaporative and runoff fluxes, resulting in increased bare soil evaporation, reduced transpiration, and higher runoff.

Plain Language Summary Satellite remote sensing, provides the ability to obtain integrated assessments of vegetation changes on the land surface. In this study, we employ the vegetation optical depth (VOD) retrievals from the NASA SMAP mission for characterizing the recent 2019-2020 Australian drought and bushfires. The results demonstrate that SMAP VOD retrievals are effective in capturing the vegetation alterations from the unprecedented fires and drought. The study also examined the associated impact of these changes on the hydrological cycle. The removal of vegetation impacted the components of evaporation, by reducing the transpiration and increasing the bare soil evaporation. The results show that the reduction in transpiration likely amplified the amount of precipitation that is converted to runoff.

1. Introduction

Bushfires are seasonal occurrences in Australia driven by a combination of factors including extreme heat, dryness, natural climate variability and human activities (Pitman et al., 2007). The most recent bushfires during the Australian summer of 2019–2020 have been unprecedented, likely due to the very dry conditions over eastern Australia in the past 2 years resulting from the absence of a La Nina event (King et al., 2020). The Murray-Darling basin in particular, has experienced persistent droughts in the last several years with the summer of 2019–2020 being the driest and hottest period on record. Roughly 25 million acres, including more than 21% of the Australian forests, have burned from the 2019 to 2020 fires (Boer et al., 2020). The fires grew in size during September and October of 2019 and caused major destruction during the Australian summer months until the heavy rain events in mid-January and early February of 2020.

Plant physiology and growth are directly affected by soil water deficit conditions and disturbances such as fires. Monitoring vegetation changes, therefore, can help to characterize and diagnose such conditions on the land surface. Remote sensing measurements, particularly from multispectral optical and thermal imagers are typically used to provide spatial characterization of vegetation changes on the land surface from

geophysical retrievals such as leaf area index (LAI), fraction of photosynthetically active radiation, and normalized difference vegetation index (Houborg et al., 2015). The high-resolution (1 km and finer) nature of these observations makes them particularly valuable for fire monitoring, but they are subject to some sensing limitations. For example, cloud cover often limits the spatial coverage of the data from optical and thermal sensors. While these measurements provide valuable information on the burned areas, any gap in their spatial coverage may limit their suitability for rapid assessment of ecosystem impacts and structural changes to vegetation.

Microwave radiometry, on the other hand, allows for all-weather observations of the land surface in large parts of the 1–40 GHz spectral region. Traditionally, microwave measurements are used for retrieving soil moisture as low-frequency microwave signals are sensitive to changes in soil wetness (Njoku & Entekhabi, 1996). The microwave emission from the soil is also attenuated by the vegetation and combines with direct and reflected vegetation emission into the signal measured above the canopy. Unlike soil moisture or temperature, the attenuation by the vegetation has opposing effects on horizontal and vertical polarized emission. This depolarizing effect can be exploited to retrieve the vegetation optical depth (VOD) based on first-order radiative transfer equations (Meesters et al., 2005). Recent studies have explored the use of VOD as an analog of above canopy biomass in applications of drought, dryland vegetation dynamics, and deforestation (Andela et al., 2013; Konings & Gentine, 2017; van Marle et al., 2016). A key limitation of current passive microwave VOD retrievals is their coarse spatial resolution of about 25–40 km. However, VOD and soil moisture retrievals at finer spatial scales (~9 km) have been produced from satellites such as the Soil Moisture Active Passive (SMAP) mission, exploiting the oversampling of the antenna overpasses to improve the resolution (Chaubell et al., 2016). In addition, studies have shown that higher resolution VOD retrievals can be obtained from active sensors such as the C-SAR instrument onboard Sentinel-1 (Albergel et al., 2018; Hajj et al., 2019), which is promising for developing estimates of vegetation changes from microwave radiometry. The more continuous temporal information from microwave sensors, in particular, can be exploited for modeling the fire impacts on regional hydrology and ecosystems.

Vegetation indices such as VOD encompass and represent the impacts of vegetation stress due to various environmental factors, including drought and fires. The Australian summer of 2019–2020, therefore, present an interesting case study to employ microwave sensor-based vegetation retrievals for characterizing the vegetation changes on land surface and for examining their impacts on hydrological states and fluxes. Though the coarse resolution of the microwave measurements is typically prohibitive for the detection of small fires, the large scale nature of the 2019–2020 Australian bushfires also makes the use of microwave data more relevant. In this study, we employ the VOD retrievals from SMAP and examine their effectiveness for detecting vegetation variations from the Australian bushfires and drought. The SMAP VOD retrievals are then assimilated within a dynamical phenology model to examine the impact of the vegetation changes on energy and water fluxes and land surface states. The results of the SMAP VOD assimilation are also contrasted against a model run that assimilates the optical sensor-based LAI estimates from the Moderate Resolution Imaging Spectroradiometer (MODIS) instrument. The impact of assimilating VOD and LAI is assessed by comparing to a number of independent measurements and data products of evapotranspiration (ET), runoff (Q), and soil moisture.

2. Approach

2.1. Model Configuration

The study is focused on southeast Australia, with an areal extent of 25–40°S and 140–154° at 0.01° spatial resolution (Figure S1). The Noah-MP land surface model (version 3.6; Niu, 2011; Yang et al., 2011) forced with hourly meteorology from NASA's Modern Era Retrospective-Analysis for Research and Applications version 2 (MERRA2; Gelaro et al., 2017) is used for modeling and data assimilation (DA) integrations. More details of the model configuration are provided in Supporting Information S1.

Noah-MP includes a dynamical phenology model that allows for the assimilation of vegetation indices from remote sensing. In a recent study, Kumar et al. (2020) demonstrated the beneficial impact of assimilating X-, C-, and L-band VOD retrievals for improving water and carbon fluxes and states over the continental United States. Here, we employ a similar setup over southeast Australia. The model and DA integrations cover the

period of April 2015 to February 2020, representing the time period when the SMAP L-band observations are available.

2.2. DA of SMAP VOD and MODIS LAI

In this study, we employ the assimilation of the enhanced, 9 km Level 2 VOD retrievals from SMAP (SPL2SMP_E; Chaubell et al., 2016) and the 500-m MCD15A2H collection six LAI data (Myneni, 2015) from the MODIS sensors aboard NASA's Terra and Aqua satellites. The details of these data products are provided in Supporting Information S2 and S3. The assimilation integrations employ an ensemble size of 20 with perturbations applied to a number of meteorological and model state variables. Additional details of the DA setup are provided in the Supporting Information S1.

A direct independent evaluation of the utility of assimilation over the burned areas and drought locations of 2019–2020 is difficult given the lack of sufficient, colocated reference measurements over those areas. Instead, the article examines the impact of VOD assimilation in influencing the water budget terms of ET, Q, and soil moisture, during the entire model integration time period of 2015–2020. The ET simulations are compared against the gridded, 5 km daily Atmosphere-Land Exchange Inverse (ALEXI; Anderson et al., 2007) and the in situ eddy-covariance ET measurements from the OzFlux network (http://www.ozflux.org.au). The Q estimates are evaluated against the Australian Bureau of Meteorology (BoM) Hydrologic Reference Station streamflow data (http://www.bom.gov.au/water/hrs/). The impact of DA on simulated soil moisture states is evaluated using (1) the BoM high resolution soil moisture analysis called JASMIN (Joint UK Land Environment Simulator [JULES]-based Soil Moisture Information; Vinodkumar & Dharssi, 2019), and (2) the in situ soil moisture measurements available from the International Soil Moisture Network (ISMN; Dorigo et al., 2011). Note that the high-resolution JASMIN data is used by the BoM for characterizing the spatial variability of soil moisture related to fire occurrences (Vinodkumar & Dharssi, 2017). More details on these datasets are provided in Supporting Information S4.

3. Results

Figure 1 shows false color images of Bands M11-I2-I1 from the Visible Infrared Imaging Radiometer Suite (VIIRS) onboard the Suomi National Polar-orbiting Partnership (NPP) spacecraft and the anomalies in SMAP VOD for January 22 (selected based on the maximum orbital coverage of NPP and SMAP) for years 2017–2020 over southeast Australia. The VIIRS image for January 22, 2020 shows the impact of the 2019–2020 bushfires. The burn scars from the fire are seen as dark red in the 2020 map, whereas green color (representing vegetated land) is observed over those same areas in prior years, when fire impacts were small. The daily SMAP VOD anomalies are computed by subtracting the monthly mean climatology values from the daily SMAP VOD estimates. The anomalies thus represent the daily deviations from the mean seasonal cycle. Similar to the features in the VIIRS maps, the VOD anomalies are generally positive in 2017, 2018, and 2019, indicating the increased vegetation activity during a typical summer season (compared to the climatological baseline of 2015–2020). In contrast, significant negative anomalies are observed in 2020 over large portions of eastern New South Wales (NSW) and Victoria. These areas with significant negative anomalies in SMAP VOD represent the combined impact of the drought and burned scars. In particular, the spatial patterns of the negative VOD anomalies in January 22, 2020 are matched well with the areas of burned scars in the corresponding VIIRS map (Figure 1).

As the VOD anomalies in SMAP also include the general influence of water stress on vegetation, the effectiveness of SMAP data in specifically capturing the burn scar features is quantitatively evaluated by comparing to the Terra Aqua combined burned area product (MCD64A1, collection 6), which derives a burn sensitive vegetation index using the surface reflectance information from MODIS (Giglio et al., 2018). Categorical metrics of accuracy and kappa coefficient (described in the Supporting Information Section S5) are used to compute the spatial similarity of the burn scar estimates from MCD64A1 (upscaled to 9 km) and the SMAP VOD anomalies for January 2020. The domain-averaged accuracy (which considers both the correct detections and nonevents) of the SMAP VOD anomaly maps is 0.94, whereas the kappa-coefficient is 0.46. While the accuracy level is high, the kappa-coefficient indicates a moderate level of agreement with

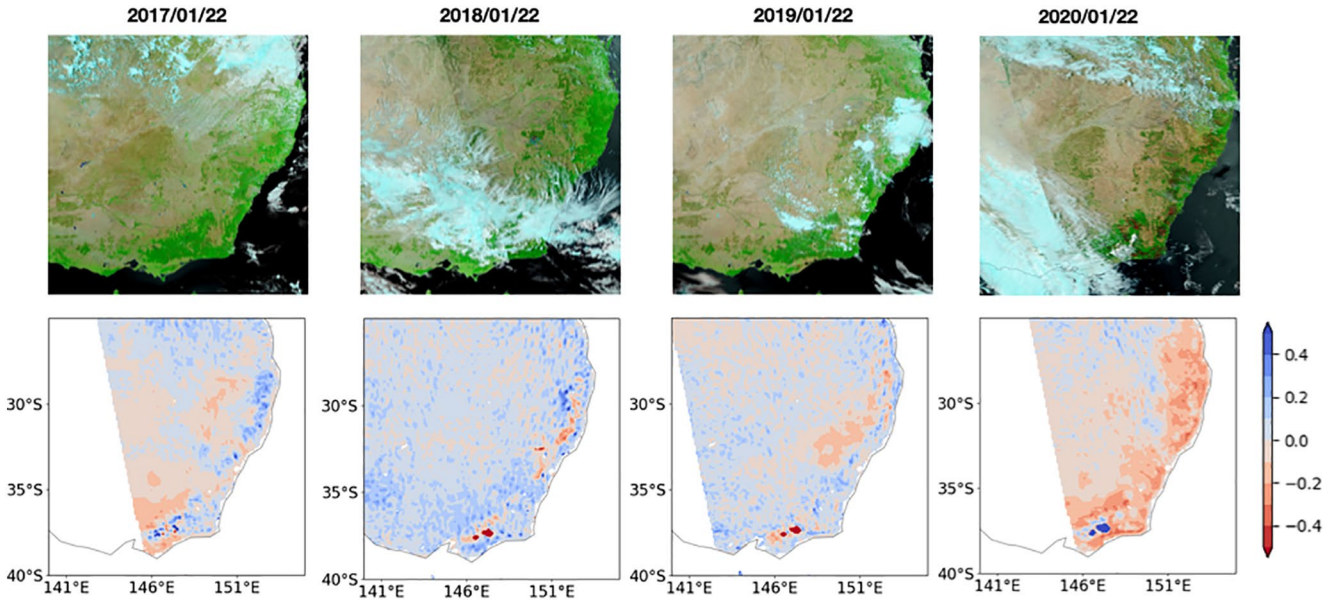

Figure 1. False color images of Bands M11-I2-I1 from VIIRS/Suomi NPP over Southeast Australia (top row) and maps of anomalies in SMAP VOD (−) for January 22 from years 2017 to 2020 (bottom row). The burn scars from the 2019–2020 Bushfires are visible in dark red color in the January 22, 2020 image, whereas those areas appear green representing vegetated land in prior years. These VIIRS/Suomi NPP images are obtained from worldview.earthdata.nasa.gov. NPP, National Polar-orbiting Partnership; SMAP, Soil Moisture Active Passive; VIIRS, Visible Infrared Imaging Radiometer Suite; VOD, vegetation optical depth.

MCD64A1 (Landis & Koch, 1977). It was also noted that 33.8% of the pixels with a VOD anomaly lower than −0.2 are also classified as burned area by MCD64A1. These quantitative evaluations along with the visual comparisons in Figure 1 confirm that the SMAP VOD estimates encompass the vegetation disturbance features of the Australian bushfires of 2019–2020.

The comparisons in Figure 1 also suggest that VOD anomalies include vegetation stress impacts beyond the specific burn scar features, particularly over the forested regions. This is due to the combined influence of the fire, extreme drought, and dry conditions of 2019–2020 on vegetation. To examine the impact of these vegetation disturbances, we employ the SMAP VOD data for DA within the Noah-MP land surface model. The assimilation setup is used to extend the information on fire and drought related vegetation changes from SMAP to land surface moisture conditions and fluxes such as ET and Q.

Figures 2a and 2b show the changes in root mean square error (RMSE) and Pearson correlation coefficient (R) of ET between DA and open loop (OL; model run without assimilation) integrations using ALEXI as the reference. The comparisons to ALEXI indicate that assimilation of VOD and LAI is beneficial in improving ET estimates, leading to reductions in RMSE and increases in the temporal correlation over most parts of the domain. RMSE improvements as large as 25 W/m^2 and increase in R as high as 0.28 are obtained from the vegetation DA configurations. Particularly strong improvements are observed over croplands in NSW and Victoria provinces. In both ALEXI and OzFlux comparisons, the improvements from VOD DA are comparable to those from LAI assimilation, confirming that the use of VOD is an effective option for incorporating information on vegetation conditions. Similar to the findings of the previous study that demonstrated the use of LAI and VOD for DA (Kumar et al., 2020, 2019), most of these improvements are related to the changes in vegetation seasonality introduced by DA (not shown). Figures 2c and 2d show the RMSE and Bias in ET compared to the in situ OzFlux ET measurements. These comparisons also confirm the beneficial impact of VOD and LAI assimilation for improving the accuracy of ET estimates. At all locations except Wombat State Forest, VOD assimilation leads to small, but statistically significant improvements in ET RMSE and Bias. When seasonally stratified, larger improvements (up to 15 W/m^2 at a monthly scale) are observed during the Australian summer time period at these locations (not shown). Both these comparisons confirm that the enhancements in vegetation representation from SMAP VOD assimilation also translate to improvements in simulated ET.

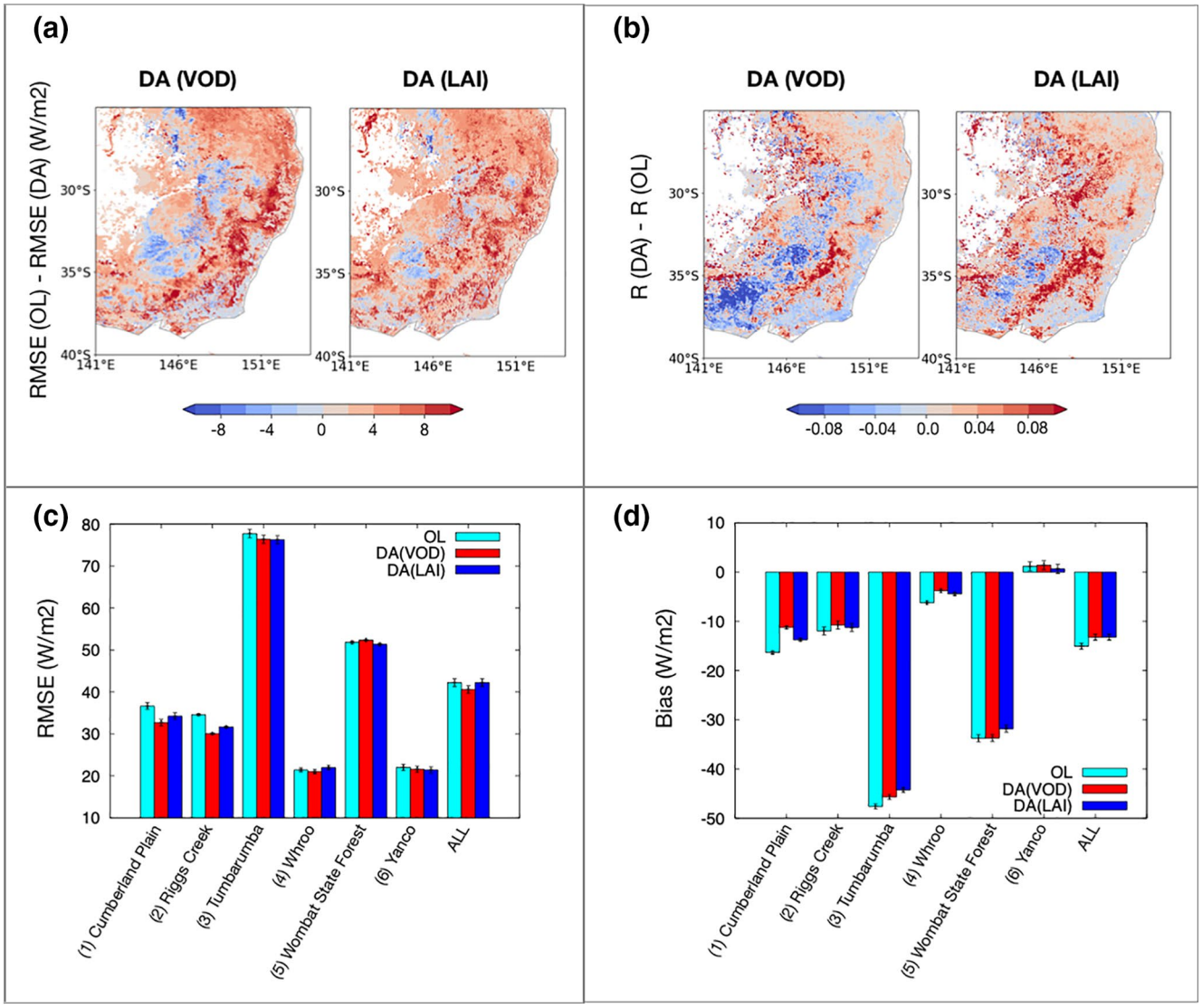

Figure 2. Impact of VOD and LAI assimilation on simulated ET compared to ALEXI and OzFlux measurements. Panel (a) shows the RMSE difference (RMSE(OL) − RMSE(DA), in units of W/m^2) and panel (b) shows R difference (expressed as R(DA) − R(OL)) compared to ALEXI during 2015–2020. Panels (c) and (d) show the RMSE and Bias (in units of W/m^2 with 95% confidence intervals shown as whiskers) of ET, respectively, from the OL and DA simulations compared to the in situ measurements from the OzFlux network during January 2015 to February 2020. ALEXI, Atmosphere-Land Exchange Inverse; DA, data assimilation; ET, evapotranspiration; LAI, leaf area index; OL, open loop; RMSE, root mean square error; VOD, vegetation optical depth.

Figure 3 shows the impact of VOD and LAI assimilation on the Q. Monthly averaged Q simulations were integrated across each of the catchments where streamflow observations are available. Using monthly total runoff as a proxy for streamflow is a valid assumption, since concentration times of small catchments are generally on the order of days (Chow, 1964). The impact of DA on monthly Q is quantified using normalized information contribution (NIC) metric (Kumar et al., 2009) for R and Nash-Sutcliffe Efficiency (NSE), described in Supporting Information S5. These normalized metrics are used because the magnitude of the NSE varies significantly across different basins. Overall, both VOD and DA assimilation generate small, but beneficial impacts on streamflow in most parts of the domain, whereas some degradations are noted over locations in Victoria and northern parts of the domain. Similar to the ET evaluation, the Q comparisons in Figure 3 indicate comparable impacts from VOD and LAI assimilation. At a domain averaged scale, the average NIC (R) values are 0.06 and 0.08, for VOD and LAI DA, respectively. For NIC NSE, VOD DA pro-

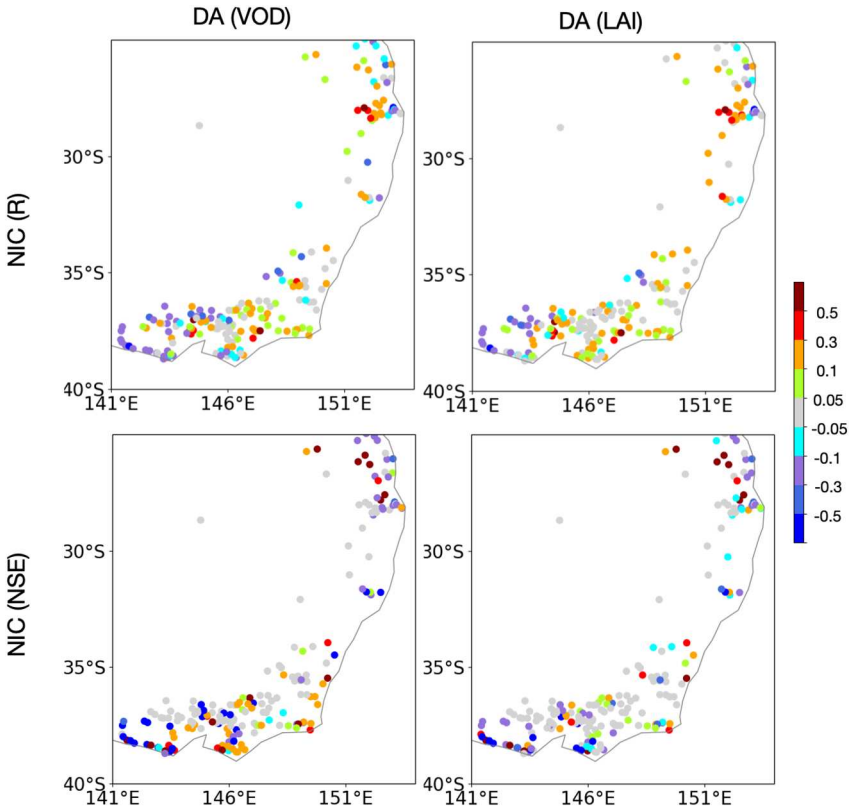

Figure 3. Impact of VOD and LAI assimilation on simulated streamflow using the Bureau of Meteorology Hydrologic Reference Station data as the reference during January 2015 to February 2020. The top and bottom rows represent the NIC in R and NSE, respectively, whereas the left and right columns represent the VOD and LAI DA runs, respectively. DA, data assimilation; LAI, leaf area index; NIC, normalized information contribution; NSE, Nash-Sutcliffe Efficiency; VOD, vegetation optical depth.

vides a domain averaged estimate of 0.12, whereas LAI DA leads to a slightly smaller, 0.09 domain averaged estimate.

The changes in anomaly *R* between DA and OL integrations for surface and root zone soil moisture are compared against the JASMIN estimates (Figure S2). Here, surface and root zone soil moisture values are defined as the soil moisture content for the top 10 cm and 1 m of the soil column. The root zone soil moisture is computed as a suitably weighted average (based on soil thickness of the individual layers) of the profile soil moisture. Anomaly *R* values are computed as the correlation of daily anomalies (of model and JASMIN data) computed by subtracting daily soil moisture values from the respective monthly mean values (across 2015–2020). SMAP VOD and MODIS LAI assimilation has minimal impacts on the surface soil moisture (Figure S2). On the other hand, assimilation leads to significant improvements in root zone soil moisture. Though there are some patterns of degradation in the northern part of the modeling domain, the evaluation against JASMIN shows significant improvements in the eastern and southern parts of the domain, areas where cropland is the dominant vegetation type. The patterns of improvements and degradations are very similar between the VOD and LAI DA integrations.

When compared to the in situ measurements from the ISMN data, the average anomaly *R* values across the 18 stations for the OL surface and root zone soil moisture are 0.67 and 0.30, which improves to 0.69 and 0.39 with VOD DA. Similar impacts are also obtained with MODIS LAI assimilation, where the average anomaly *R* improves to 0.68 and 0.41, for surface and root zone soil moisture, respectively. These results are consistent with the patterns in the JASMIN comparison, where larger improvements are observed for root zone soil moisture compared to the surface soil moisture (over the NSW region).

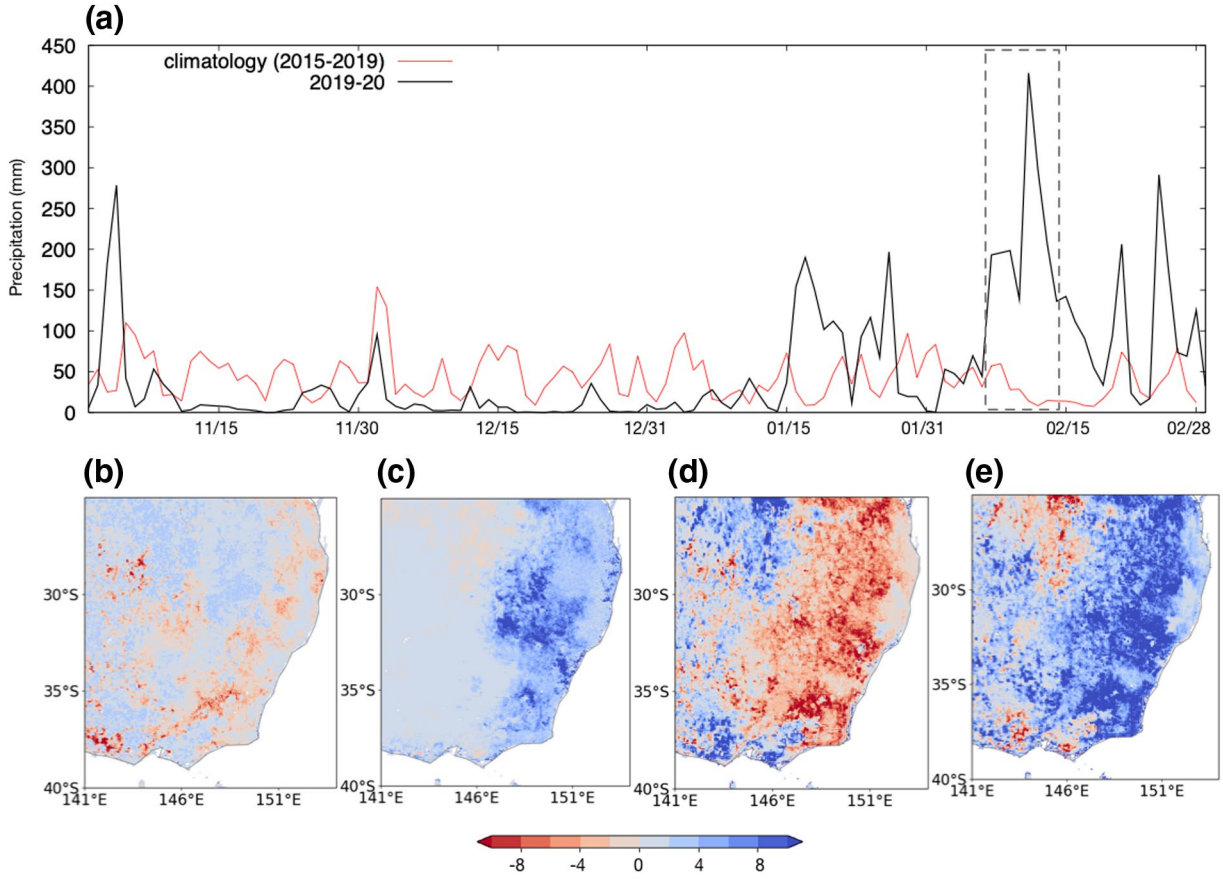

Figure 4. Time series of domain averaged precipitation in units of mm (panel a). The bottom panel shows the percentage change in (b) ET and (c) Q between the VOD DA and VOD-CLIMO DA runs during February 7–14, 2020. Panels (d) and (e) show the percentage change in the transpiration and bare soil evaporation partitions, respectively, between the VOD DA and VOD-CLIMO DA runs. DA, data assimilation; ET, evapotranspiration; VOD, vegetation optical depth.

The evaluations presented above confirm the beneficial role of VOD assimilation for improving land surface states and fluxes, though they do not necessarily focus on the impacts of the 2019–2020 fires and drought. To contrast and isolate the impact of vegetation disturbance in the 2019–2020 season, an additional integration is conducted where the daily climatological conditions across years 2015–2019 are assimilated into the Noah-MP model (VOD-CLIMO DA) during the 2019–2020 summer time period. The daily SMAP VOD climatology is generated by averaging the retrievals for each day without including the 2019–2020 Australian summer time period. The differences between the VOD DA and VOD-CLIMO DA runs are the vegetation changes from 2019 to 2020 summer alone, as factors such as the driving meteorology are identical in these two integrations. The water budget fluxes estimates from VOD DA and VOD-CLIMO DA are compared to quantify the influence of fire and drought-induced vegetation disturbances from 2019 to 2020.

The top panel of Figure 4 shows a time series of domain averaged precipitation during November–February of 2019–2020 and the climatological precipitation (across years 2015–2019). The precipitation comparison indicates that the summer of 2019–2020 is abnormally dry compared to other years. The dry spell is ultimately ended by the arrival of heavy precipitation in mid-January and February. The average precipitation for the November–January of 2019–2020 over the model domain is 30 mm, compared to the climatological average of 46 mm (across 2015–2019). The bottom row of Figure 4 presents an example of the impact of vegetation changes on the modeled hydrological cycle from fire and drought related vegetation disturbances, during a week of February 7–14, when heavy precipitation events occurred in NSW. The percentage change in ET and Q between the VOD DA and VOD-CLIMO DA runs is shown in Figures 4b and 4c. The vegetation disturbance in the 2019–2020 season has a significant impact on ET and Q, particularly over the eastern parts of the domain. The removal of vegetation leads to reduced ET and increased Q, with Q increasing by as

much as 14% in certain parts of the domain. In spite of the significant dry spell in the months leading up to January 2020, the precipitation onset leads to significant Q generation, contributed by the absence of vegetation and the lack of significant transpiration. These quantifications confirm the role of the decreased vegetation presence in the flooding that occurred in NSW in response to precipitation events of early February.

In addition, the partition of ET into its components of transpiration (T) and bare soil evaporation (E) is significantly different in 2019–2020. Figures 4d and 4e show the percentage change in the fractional partition of ET into T and E between the VOD DA and VOD-CLIMO DA runs (using VOD-CLIMO DA as the basis). The fractional partition of T reduces significantly, whereas E increases. With less vegetation surviving the 2019–2020 fire-drought season than in typical years, the increase in ET is mainly driven by soil evaporation rather than transpiration. These changes in the ET partition also contributes to increased Q generation, as seen in the results of Figure 4c. The changes in the ET, T, E, and Q patterns shown in Figure 4 provide a representative example of the important influence of fire and drought driven vegetation disturbance in the water fluxes and their partitioning.

4. Summary and Conclusions

Remote sensing based information is critical for monitoring and assessing the impact of vegetation changes from droughts and fires. Typically, optical or thermal infrared sensors are used to develop assessments of burn scars, partly because of the fine spatial resolution of their measurements. Though coarser in their spatial resolution, passive microwave-based estimates are nearly all weather and could be used to improve the spatio-temporal coverage of optical vegetation remote sensing estimates. VOD, an indicator of above ground biomass and vegetation stress, is available from passive microwave radiometry. In this study, we examine the utility of VOD retrievals from the NASA SMAP mission in characterizing the recent 2019–2020 Australian bushfires and drought. The large-scale nature of these fires and the drought allow the use of passive microwave remote sensing data for characterizing the impact of vegetation disturbances on hydrological states and fluxes, despite their coarse spatial resolution.

The results in this article show that the SMAP VOD retrievals capture the vegetation stress conditions from the 2019 to 2020 Australian fires and drought. The quantitative comparisons demonstrate that the spatial patterns of the negative SMAP VOD anomalies show moderate levels of agreement with the MODIS burned area product. The VOD retrievals are assimilated into a dynamic phenology model to further examine the impact of vegetation disturbances on water budget fluxes and states. A similar DA setup that incorporates MODIS LAI retrievals is used for developing relative assessments of the utility of microwave VOD retrievals against optical sensor-based LAI data. Comparisons against the TIR-based ALEXI data product and in situ OzFlux measurements indicate that SMAP VOD DA provides systematic improvements in the ET simulations. The beneficial impact of vegetation assimilation is also seen in the Q comparisons against the in situ streamflow measurements from the BoM. Similarly, comparisons of soil moisture fields against the high-resolution JASMIN analysis by the Australian BoM and the in situ measurements from the ISMN network also confirm the useful role of VOD retrievals, particularly for improving root zone soil moisture estimation. Positive impacts similar in magnitude in ET and soil moisture are also seen with LAI DA, confirming that the use of VOD is an effective option for incorporating impacts of vegetation changes, such as the Australian bushfires.

The results of the article show that the representation of vegetation disturbances from fires and drought also translates to significant changes in the water budget fluxes. The removal and reduction of vegetation leads to the ET regime to transition from transpiration dominated to soil evaporation dominated. The reduced vegetation presence in such circumstances leads to reduced ET and increased Q. The reduced contribution of the transpiration to ET also impacts the partitioning of precipitation into Q. The results indicate that the changes in water budget partitioning contribute to the large Q amounts that are generated in the model simulations in response to the heavy precipitation events that followed the significant dry spell and the fires during the Australian summer months of 2019 and 2020.

Overall, the results of the article demonstrate the potential of using passive microwave measurements to monitor the combined impacts of fire and drought on vegetation, particularly for large-scale disasters such as the 2019–2020 Australian bushfires and drought season. The assimilation of these measurements further

help in developing spatio-temporal assessments of the impact of fire-induced vegetation disturbances in altering the ecosystems and local hydrology. Though vegetation related changes are captured in this study through assimilation, fires can also impact the soil states, introducing water repellency to the soil. These hydrophobic processes are not represented in this study, and are left for a future work.

Data Availability Statement

Various data sets used in this study are available from the following websites: SMAP VOD—https://nsidc.org/data/smap/smap-data.html; MCD15A2H—https://lpdaac.usgs.gov/products/mcd15a2hv006/; MCD64A1—https://lpdaac.usgs.gov/products/mcd64a1v006/; OzFlux—http://www.ozflux.org.au; Bom HRS data—http://www.bom.gov.au/water/hrs/; JASMIN soil moisture—http://www.bom.gov.au/water/hrs/;VIIRS NPP imagery—https://worldview.earthdata.nasa.gov.

Acknowledgments
This research was supported by NASA Applied Sciences Grant for the Science Utilization of SMAP (SUSMAP project). Computing was supported by the resources at the NASA Center for Climate Simulation.

References

Albergel, C., Munier, S., Bocher, A., Bonan, B., Zheng, Y., Draper, C., et al. (2018). LDAS-Monde sequential assimilation of satellite derived observations applied to the contiguous US: An ERA-5 driven reanalysis of the land surface variables. *Remote Sensing*, *10*(10), 1627.

Andela, N., Liu, Y. Y., van Dijk, A. I. J. M., de Jeu, R. A. M., & McVicar, T. R. (2013). Global changes in dryland vegetation dynamics (1988–2008) assessed by satellite remote sensing: comparing a new passive microwave vegetation density record with reflective greenness data. *Biogeosciences*, *10*(10), 6657–6676. https://doi.org/10.5194/bg-10-6657-2013

Anderson, M., Norman, J., Mecikalski, J., Otkin, J., & Kustas, W. (2007). A climatological study of evapotranspiration and moisture stress across the continental U.S. based on thermal remote sensing: I. Model formulation. *Journal of Geophysical Research*, *112*(D10117), 1–17. https://doi.org/10.1029/2006JD007506

Boer, M., Resco de Dios, V., & Bradstock, R. (2020). Unprecedented burn area of Australian mega forest fires. *Nature Climate Change*, *10*, 171–172. https://doi.org/10.1038/s41558-020-0716-1

Chaubell, J., Yueh, S., Entekhabi, D., & Peng, J. (2016). Resolution enhancement of SMAP radiometer data using the Backus-Gilbert optimum interpolation technique. *2016 IEEE International Geoscience and Remote Sensing Symposium (IGARSS)* (pp. 284–287).

Chow, V. (1964). *Applied hydrology*. New York, NY: McGraw-Hill.

Dorigo, W. A., Wagner W., Hohensinn R., Hahn S., Paulik C., Drusch M., et al. (2011). The International Soil Moisture Network: A data hosting facility for global in situ soil moisture measurements. *Hydrology and Earth System Sciences*, *15*(5), 1675–1698. https://doi.org/10.5194/hess-15-1675-2011

Gelaro, R., McCarty, W., Suárez, M. J., Todling, R., Molod, A., Takacs, L., et al. (2017). The Modern-Era Retrospective Analysis for Research and Applications, version 2 (MERRA-2). *Journal of Climate*, *30*(14), 5419–5454. https://doi.org/10.1175/JCLI-D-16-0758.1

Giglio, L., Boschetti, L., Roy, D. P., Humber, M. L., & Justice, C. O. (2018). The Collection 6 MODIS burned area mapping algorithm and product. *Remote Sensing of Environment*, *217*, 72–85. https://doi.org/10.1016/j.rse.2018.08.005

Hajj, E., Baghdadi, N., Wigneron, J.-P., Zribi, M., Algergel, C., Calvet, J.-C., &(2019). First vegetation optical depth mapping from Sentinel-1 C-band SAR data over crop fields. *Remote Sensing*, *11*(23), 2769.

Houborg, R., Fisher, J. B., & Skidmore, A. K. (2015). Advances in remote sensing of vegetation function and traits. *International Journal of Applied Earth Observation and Geoinformation*, *43*, 1–6. https://doi.org/10.1016/j.jag.2015.06.001

King, A., Pitman, A., Henley, B., Ukkola, A., & Brown, J. (2020). The role of climate variability in Australian drought. *Nature Climate Change*, *10*, 177–179. https://doi.org/10.1038/s41558-020-0718-z

Konings, A. G., & Gentine, P. (2017). Global variations in ecosystem-scale isohydricity. *Global Change Biology*, *23*(2), 891–905

Kumar, S. V., Holmes, T. R., Bindlish, R., de Jeu, R., & Peters-Lidard, C. (2020). Assimilation of vegetation optical depth retrievals from passive microwave radiometry. *Hydrology and Earth System Sciences*, *24*(7), 3431–3450. https://doi.org/10.5194/hess-24-3431-2020

Kumar, S. V., Mocko, D. M., Wang, S., Peters-Lidard, C. D., & Borak, J. (2019). Assimilation of remotely sensed leaf area index into the Noah-MP land surface model: Impacts on water and carbon fluxes and states over the continental United States. *Journal of Hydrometeorology*, *20*(7), 1359–1377. https://doi.org/10.1175/jhm-d-18-0237.1

Kumar, S. V., Reichle, R. H., Koster, R. D., Crow, W. T., & Peters-Lidard, C. D. (2009). Role of subsurface physics in the assimilation of surface soil moisture observations. *Journal of Hydrometeorology*, *10*(6), 1534–1547. https://doi.org/10.1175/2009JHM1134.1

Landis, J., & Koch, G. (1977). The measurement of observer agreement for categorical data. *Biometrics*, *33*(1), 159–174.

Meesters, A. G. C. A., De Jeu, R. A. M., & Owe, M. (2005). Analytical derivation of the vegetation optical depth from the microwave polarization difference index. *IEEE Geoscience and Remote Sensing Letters*, *2*(2), 121–123. https://doi.org/10.1109/LGRS.2005.843983

Myneni, R. (2015). MCD15A2H MODIS/Terra+Aqua Leaf Area Index/FPAR 8-day L4 Global 500m. *SIN Grid V006*. https://doi.org/10.5067/MODIS/MCD15A2H.006

Niu, G.-Y., Yang, Z.-L., Mitchell, K. E., Chen, F., Ek, M. B., Barlage, M., et al. (2011). The community Noah land surface model with multiparameterization options (Noah-MP): 1. Model description and evaluation with local-scale measurements. *Journal of Geophysical Research*, *116*(D12109), 1–19. https://doi.org/10.1029/2010JD015139

Njoku, E. G., & Entekhabi, D. (1996). Passive microwave remote sensing of soil moisture. *Journal of Hydrology*, *184*(1), 101–129.doi: https://doi.org/10.1016/0022-1694(95)02970-2

Pitman, A., Narisma, G., & McAneney, J. (2007). The impact of climate change on the risk of forest and grassland fires in Australia. *Climate Change*, *84*, 383–401. https://doi.org/10.1007/s10584-007-9243-6

van Marle, M. J. E., van der Werf, G. R., de Jeu, R. A. M., & Liu, Y. Y. (2016). Annual South American forest loss estimates based on passive microwave remote sensing (1990–2010). *Biogeosciences*, *13*(2), 609–624. https://doi.org/10.5194/bg-13-609-2016

Vinodkumar, & Dharssi, I. (2017). *Evaluation of daily soil moisture deficit used in Australian forest fire danger rating sytem (Technical Report 022). Bureau of Meteorology*.

Vinodkumar, & Dharssi, I. (2019). Evaluation and calibration of a high-resolution soil moisture product for wildfire prediction and management. *Agricultural and Forest Meteorology*, *264*, 27–39. https://doi.org/10.1016/j.agrformet.2018.09.012

Yang, Z.-L., Niu, G.-Y., Mitchell, K. E., Chen, F., Ek, M. B., Barlage, M., et al. (2011). The community Noah land surface model with multiparameterization options (Noah-MP): 2. Evaluation over global river basins, *Journal of Geophysical Research*, *116*(D12), 1–19. https://doi.org/10.1029/2010JD015140

References From the Supporting Information

Entekhabi, D., Njoku, E. G., O'Neill, P. E., Kellogg, K. H., Crow, W. T., Edelstein, W. N., et al. (2010). The Soil Moisture Active Passive (SMAP) mission. *Proceedings of the IEEE*, *98*(5), 704–716. https://doi.org/10.1109/jproc.2010.2043918

Fick, S. E., & Hijmans, R. J. (2017). WorldClim 2: New 1-km spatial resolution climate surfaces for global land areas. *International Journal of Climatology*, *37*(12), 4302–4315. https://doi.org/10.1002/joc.5086

Friedl, M., McIvera, D. K., Hodges, J. C. F., Zhang, X. Y., Muchoney, D., Strahler, A. H., et al. (2002). Global land cover mapping from MODIS: Algorithms and early results. *Remote Sensing of Environment*, *83*(1), 287–302. https://doi.org/10.1016/S0034-4257(02)00078-0

Hain, C. R., & Anderson, M. C. (2017). Estimating morning change in land surface temperature from MODIS day/night observations: Applications for surface energy balance modeling. *Geophysical Research Letters*, *44*(19), 9723–9733. https://doi.org/10.1002/2017GL074952

Hengl, T., de Jesus, J. M., MacMillan, R. A., Batjes, N. H., Heuvelink, G. B. M., Ribeiro, E., et al. (2014). SoilGrids1km—Global soil information based on automated mapping. *PloS One*, *9*(8), 1–17. https://doi.org/10.1371/journal.pone.0105992

Konings, A. G., Piles, M., Das, N., & Entekhabi, D. (2017). L-band vegetation optical depth and effective scattering albedo estimation from SMAP. *Remote Sensing of Environment*, *198*, 460–470.doi:https://doi.org/10.1016/j.rse.2017.06.037

Kumar, S., Peters-Lidard, C., Santanello, J., Harrison, K., Liu, Y., & Shaw, M. (2012). Land surface Verification Toolkit (LVT)—A generalized framework for land surface model evaluation. *Geoscientific Model Development*, *5*, 869–886. https://doi.org/10.5194/gmd-5-869-a

Kumar, S., Peters-Lidard, C. D., Tian, Y., Houser, P. R., Geiger, J., Olden, S., et al. (2006). Land information system: An interoperable framework for high resolution land surface modeling. *Environmental Modelling & Software*, *21*, 1402–1415.

Kumar, S. V., Peters-Lidard, C. D., Mocko, D., & Yudong, T. (2013). Multiscale evaluation of the improvements in surface snow simulation through terrain adjustments to radiation. *Journal of Hydrometeorology*, *14*(1), 220–232. https://doi.org/10.1175/JHM-D-12-046.1

Kumar, S. V., Peters-Lidard, C. D., Santanello, J. A., Reichle, R. H., Draper, C. S., Koster, R. D., et al. (2015). Evaluating the utility of satellite soil moisture retrievals over irrigated areas and the ability of land data assimilation methods to correct for unmodeled processes. *Hydrology and Earth System Sciences*, *19*(11), 4463–4478. https://doi.org/10.5194/hess-19-4463-2015

Liu, X., Chen, F., Barlage, M., Zhou, G., & Niyogi, D. (2016). Noah-MP-Crop: Introducing dynamic crop growth in the Noah-MP land surface model. *Journal of Geophysical Research: Atmospheres*, *121*(23), 13953–13972. https://doi.org/10.1002/2016JD025597

Mo, T., Choudhury, B. J., Schmugge, T. J., Wang, J. R., & Jackson, T. J. (1982). A model for microwave emission from vegetation-covered fields. *Journal of Geophysical Research*, *87*(C13), 11229–11237. https://doi.org/10.1029/JC087iC13p11229

Myneni, R., Hoffman, S., Knyazikhin, Y., Privette, J. L., Glassy, J., Tian, Y., et al. (2002). Global products of vegetation leaf area and fraction absorbed PAR from year one of MODIS data. *Remote Sensing of Environment*, *83*(1), 214–231. https://doi.org/10.1016/S0034-4257(02)00074-3

Rodriguez, E., Morris, C., Belz, J., Chapin, E., Martin, J., Daffer, W., &(2005). *An Assessment of the SRTM Topographic Products (Technical Report. JPL D-31639). Pasadena, CA: Jet Propulsion Laboratory*.

Xiao, Z., Liang, S., Wang, J., Xiang, Y., Zhao, X., & Song, J. (2016). Long-time-series global land surface satellite leaf area index product derived from MODIS and AVHRR surface reflectance. *IEEE Transactions on Geoscience and Remote Sensing*, *54*(9), 5301–5318. https://doi.org/10.1109/TGRS.2016.2560522